



OPEN

Calculating the force-dependent unbinding rate of biological macromolecular bonds from force-ramp optical trapping assays

Apurba Paul^{1,2,4} & Joshua Alper^{1,2,3}✉

The non-covalent biological bonds that constitute protein–protein or protein–ligand interactions play crucial roles in many cellular functions, including mitosis, motility, and cell–cell adhesion. The effect of external force (F) on the unbinding rate ($k_{\text{off}}(F)$) of macromolecular interactions is a crucial parameter to understanding the mechanisms behind these functions. Optical tweezer-based single-molecule force spectroscopy is frequently used to obtain quantitative force-dependent dissociation data on slip, catch, and ideal bonds. However, analyses of this data using dissociation time or dissociation force histograms often quantitatively compare bonds without fully characterizing their underlying biophysical properties. Additionally, the results of histogram-based analyses can depend on the rate at which force was applied during the experiment and the experiment's sensitivity. Here, we present an analytically derived cumulative distribution function-like approach to analyzing force-dependent dissociation force spectroscopy data. We demonstrate the benefits and limitations of the technique using stochastic simulations of various bond types. We show that it can be used to obtain the detachment rate and force sensitivity of biological macromolecular bonds from force spectroscopy experiments by explicitly accounting for loading rate and noisy data. We also discuss the implications of our results on using optical tweezers to collect force-dependent dissociation data.

The weak non-covalent bonds that constitute protein–protein and protein–ligand interactions underlie nearly all cellular functions¹. For example, the physical chemistry of protein–protein interactions is fundamental to the molecular mechanisms of the cytoskeleton². Kinesin and dynein motor proteins precisely regulate and coordinate changes in motor–filament binding affinity as a function of their mechanochemical cycles as they walk along microtubules, and quantitative models of motors must explicitly account for the effects of external forces (F) on the filament unbinding rate constant ($k_{\text{off}}(F)$)². Beyond motors, examples of force-dependent unbinding rate constants are ubiquitous in biological systems, including cell–cell adhesion^{3–5}, mechanotransduction^{6,7}, DNA polymerases and helicases^{8,9}, membrane-surface adhesion¹⁰, selectin–ligand^{11,12}, and antibody–antigen complexes^{13–15}.

Weak non-covalent bonds between biological macromolecules can be classified into three principal categories¹⁶. Slip bonds have a lifetime that decreases with the increasing applied force¹⁷. Catch bonds have a lifetime that increases with applied force^{10,18}. Ideal bonds have a lifetime that is independent of applied force¹⁰. Many biomolecular interactions have been characterized using single-molecule techniques and understood in the context of these models.

Single-molecule force spectroscopy experiments involving the force-dependent unbinding of motor proteins¹⁹, microtubule- and actin-associated proteins^{20–22}, focal adhesion proteins^{23,24}, and many others^{25–27}, are commonly done using optical tweezers to apply a constant (i.e., a step function, or force jump, in time) or linearly increasing force²⁸ (e.g., a force ramp starting a zero upon binding and increasing until detachment) to the molecules (Fig. 1a). Data calculated from force spectroscopy traces frequently include the bound time and unbinding force (Fig. 1b). For example, recent single-molecule experiments on cytoplasmic dynein motor proteins show both

¹Department of Physics and Astronomy, Clemson University, Clemson, SC, USA. ²Eukaryotic Pathogens Innovation Center, Clemson University, SC, Clemson, USA. ³Department of Biological Sciences, Clemson University, Clemson, SC, USA. ⁴Department of Electrical Engineering, University of Notre Dame, Notre Dame, IN, USA. ✉email: alper@clemson.edu

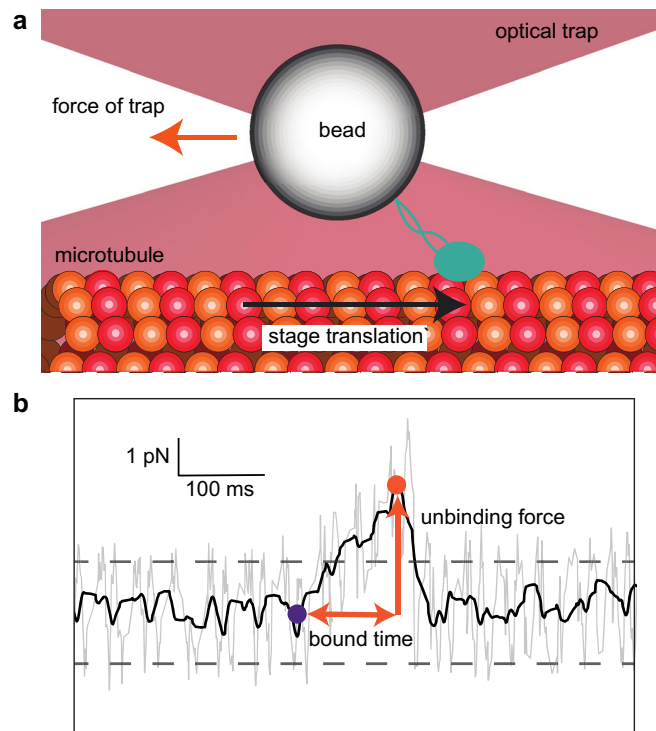


Figure 1. Microtubule-associated protein dissociation from a microtubule in a force-ramp optical trapping assay. **(a)** Schematic of a microtubule (red and orange circles) bound to a stage that moves (with velocity, v , black arrow) and pulls a bead conjugated to a microtubule-associated protein (MAP, green) out of the trap center (with effective stiffness of the trap and MAP, κ). The force that the trap exerts on the bead (orange arrow) increases at a rate of $f = \kappa v$ (thus $F(t) = ft$) until the MAP stochastically unbinds from the microtubule, which causes it to return to the trap center. The force-dependent unbinding rate constant, $k_{\text{off}}(F)$, governs the biophysics of unbinding. **(b)** A typical force spectroscopy trace (gray = raw data, black = filtered data) from a force-ramp optical tweezer assay showing the force as a function of time during a biological macromolecular binding (initial binding, purple dot) and unbinding (final unbinding, orange dot) event. The unbinding force and bound times (orange arrows) are used to determine $k_{\text{off}}(F)$ for the MAP-microtubule interaction. An event is “detected” when the filtered signal exceeds 5-times the standard deviation of the noise (dashed lines). This panel was graciously provided by Dr. Ashok Pabbathi under a CC BY open access license.

catch bond and slip-ideal bond behaviors^{29,30} and that kinesin exhibits force-dependent stepping velocities and microtubule unbinding rates that are a function of force direction³¹. Multiple techniques exist to analyze this data³², including a recent work extending classical analysis techniques to characterize motor proteins pulling cargo from a stationary optical trap³³.

This report presents a cumulative distribution function approach to these analysis techniques that unambiguously characterizes biological macromolecular slip, ideal, and catch-bond force-dependent unbinding. It deconvolves the effects of how the experiment was performed with the unbinding force and time probably distributions, and it accounts for noise-based detection limits. We demonstrate the method’s ability to extract the molecular parameters from force-ramp optical trapping assay data, including the zero-force unbinding rate constant, force-dependent rate constants, and force sensitivities, using simulated data from various bond types.

Theory

Consider a non-covalent, biological macromolecular bond, like one that underlies a protein–protein interaction. Based on classical thermodynamic models, the system has an unbinding constant, k_{off} , at quasi-thermodynamic equilibrium (for bonds subject to loading that is slow compared to the timescales of force equilibrium and thermal fluctuations). In the absence of force and in a dilute solution, the average lifetime of a protein–protein interaction bond is the inverse of its unbinding constant, $\langle \tau_{\text{off}} \rangle = 1/k_{\text{off}}$. We consider an ensemble with N independent bonds formed at $t = 0$, of which $n(t)$ of them remain bound at time t . The unbinding kinetics of the ensemble, assuming bonds do not reform after breaking, are

$$\frac{dn}{dt} = -k_{\text{off}}(F(t))n. \quad (1)$$

In general, the unbinding constant $k_{\text{off}}(F(t))$ is a function of the force applied to the bond, and we consider the case that each bond is subject to a time-varying external force, $F(t)$, e.g., as exerted by an optical tweezer.

By separating the variables and integrating Eq. (1), we find a cumulative distribution-like function for $n(t)$,

$$n(t) = Ne^{-\int k_{\text{off}}(F(t))dt}. \quad (2)$$

The functional form of $k_{\text{off}}(F(t))$ depends on the bond type and how force changes with time, e.g., a linearly increasing force ramp ($F(t) = ft$) where f , the time rate of change of applied force, is constant. By applying models that relate the unbinding constant and force, we can complete the integration and obtain a functional form for the number of unbroken bonds as a function of time, $n(t)$.

Slip bonds. The unbinding constant of a slip bond, $k_{\text{off},s}$, increases exponentially with force per Bell's model¹⁷

$$k_{\text{off},s}(F(t)) = k_{0,s}e^{\frac{F(t)}{F_s}}, \quad (3)$$

where $k_{0,s}$ is the force-free unbinding constant and F_s is the force sensitivity of the slip bond. Slip bonds with small F_s as compared to the applied load are more force-sensitive than those with large F_s . Thus, for a linearly increasing force ramp,

$$k_{\text{off},s}(t) = k_{0,s}e^{\frac{ft}{F_s}}. \quad (4)$$

Therefore, Eq. (2) is

$$n(t) = Ne^{-\int k_{0,s}e^{\frac{ft}{F_s}} dt} = Ne^{-\frac{F_s k_{0,s}}{f} \left(e^{\frac{ft}{F_s}} - 1 \right)}, \quad (5)$$

for a slip bond, as was previously similarly derived³⁴.

However, the fastest unbinding events may not be observable above experimental noise or may not be within the time sensitivity of force spectroscopy data. For example, binding/unbinding events in a linear force ramp experiment (Fig. 1b) are only observable if the force at the time of dissociation is significantly larger than the amplitude of the thermal fluctuations of a bead in the trap times the effective stiffness of the trap, F_{noise} . Therefore, we introduce a time scale, t_0 , representing the shortest observable event in a linear force ramp experiment, $t_0 = F_{\text{noise}}/f$. Thus, the total number of observable binding events is

$$n_0 = Ne^{-\frac{F_s k_{0,s}}{f} \left(e^{\frac{ft_0}{F_s}} - 1 \right)}. \quad (6)$$

Due to the experimental noise, this analysis suggests that

$$N - n_0 = n_0 e^{\frac{F_s k_{0,s}}{f} \left(e^{\frac{ft_0}{F_s}} - 1 \right)} - n_0 = n_0 \left(e^{\frac{F_s k_{0,s}}{f} \left(e^{\frac{ft_0}{F_s}} - 1 \right)} - 1 \right) \quad (7)$$

unbinding events occur in a time less than t_0 and are missing from the observable dataset. Thus, to characterize the physical properties of a slip bond, one can record the number of bonds that remain unbroken as a function of time, and fit the data to

$$n(t) = n_0 e^{-\frac{F_s k_{0,s}}{f} \left(e^{\frac{ft}{F_s}} - e^{\frac{ft_0}{F_s}} \right)}, \quad (8)$$

where the slip bond characteristics, F_s and $k_{0,s}$, are the fitting parameters. $n(t)$, and therefore F_s and $k_{0,s}$, strongly depend on the loading rate, f , of the experiment. While $f = \kappa v$ can be controlled by changing with the stage translation rate, v , in a fixed-beam optical tweezer assay (Fig. 1a) or trap translation in a fixed-stage optical tweezer assay, and the trap stiffness, κ_{trap} , the loading rate is additionally complicated by the finite stiffness of the system, including linking molecules, κ_{system} , where $\frac{1}{\kappa} = \frac{1}{\kappa_{\text{trap}}} + \frac{1}{\kappa_{\text{system}}}$.

Ideal bonds. The unbinding constant of an ideal bond, $k_{\text{off},i}$, does not change with force. Hence, even when the applied force changes with time, the unbinding constant remains constant. In that case, the unbinding constant is $k_{\text{off},i}(t) = k_{0,i}$ and Eq. (2) becomes

$$n(t) = Ne^{-k_{0,i}t} \quad (9a)$$

or

$$n(t) = n_0 e^{-k_{0,i}(t-t_0)}, \quad (9b)$$

where n_0 is the total number of observable binding events. $n(t)$ is not a function of the loading rate, f , in the ideal bond case, and ideal bonds are special cases of slip bonds where the bond is entirely insensitive to force, i.e., for the limit when $F_s \rightarrow \infty$ (Supplementary Information).

Slip-ideal bonds. Recent data suggests that certain protein-protein interactions may be best modeled as a slip-ideal bond³⁰. The force-dependent unbinding constant of a slip-ideal bond, $k_{\text{off},s-i}(F(t))$, increases exponen-

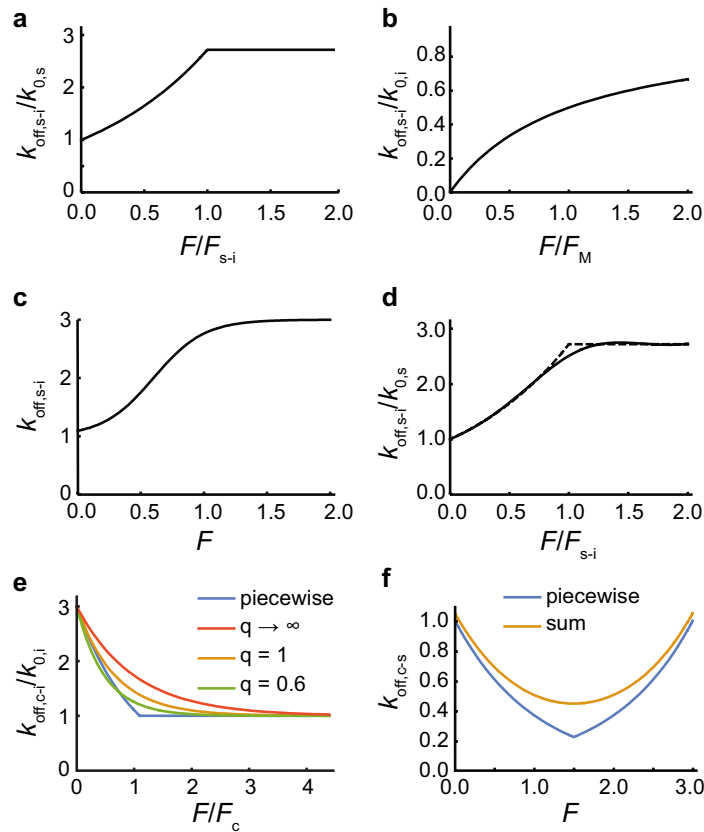


Figure 2. Analytical models for the force-dependent unbinding constant of slip-ideal, catch-ideal, and catch-slip bonds. **(a)** The piecewise function that explicitly models a slip-ideal bond (Eq. (10)) normalized by the unbinding constant at zero force and plotted as a function of force normalized by the slip-ideal transition force for the case of $F_{s-i} = F_s$. **(b)** A Michaelis–Menten or Langmuir absorption-like approximation of the slip-ideal bond (equation (S1)) normalized by the ideal bond’s unbinding constant and plotted as a function of the force normalized by the Michaelis constant-like characteristic force. **(c)** A sigmoidal approximation of a slip-ideal bond (equation (S3)) where $k_a = 2$, $k_b = 1$, $F_a = \frac{1}{5}$ and $F_b = \frac{3}{5}$. **(d)** A rational interpolation approximation (equation (S5), *solid line*) of the piecewise function from panel **(a)** (*dashed line*) for a slip-ideal bond with $F_{s-i} = F_s = 1$, which is equivalent to $\beta = 1$ (Supplementary information), normalized by the slip-bond unbinding constant, and plotted as a function of the force normalized by the characteristic force of the slip ideal transition, i.e., $\frac{k_{\text{off},s-i}(F(t))}{k_{0,s}} = \frac{1 - 0.42 \frac{F}{F_{s-i}} + 0.27 \left(\frac{F}{F_{s-i}}\right)^2}{1 - 1.35 \frac{F}{F_{s-i}} + 0.84 \left(\frac{F}{F_{s-i}}\right)^2 - 0.15 \left(\frac{F}{F_{s-i}}\right)^3}$ per Table S1. **(e)** The piecewise function (*blue*, Eq. (13)) that explicitly models a catch-ideal bond, as well as functional approximations of that function (*red, yellow, green*, Eq. (20)), normalized by the characteristic slip-bond unbinding constant and plotted as a function of force normalized by the force of the catch-bond for the representative case of $k_{0,c} = 3k_{0,i}$. **(f)** The piecewise function (*blue*, Eq. (16)) and sum formulation (*yellow*, Eq. (17)) of a model for the force-dependent unbinding constant of the catch-slip bond. In both cases, we used $k_{0,c} = 1 \text{ s}^{-1}$, $F_c = 1 \text{ pN}$, $k_{0,s} = 0.05 \text{ s}^{-1}$, and $F_s = 1 \text{ pN}$ as an example set of parameters. Given these parameters, $F_{c-s} = 1.50 \text{ pN}$.

tially with force per Bell’s model¹⁷ up to the slip-ideal transition force, F_{s-i} , beyond which, it behaves as an ideal bond (Fig. 2a). Therefore, the simplest mathematical model for the force-dependent unbinding constant of a slip-ideal bond is a piecewise function,

$$k_{\text{off},s-i}(F(t)) = \begin{cases} k_{0,s} e^{\frac{F(t)}{F_s}} & F < F_{s-i} \\ k_{0,i} & F \geq F_{s-i} \end{cases} \quad (10a)$$

While there appear to be four independent parameters: the ideal bond’s unbinding constant, the slip bond’s unbinding constant and force sensitivity, and the slip-ideal transition force, F_{s-i} , they are related by $k_{0,i} = k_{0,s} e^{\frac{F_{s-i}}{F_s}}$, or equivalently $F_{s-i} = \alpha F_s$ where $\alpha = \ln \frac{k_{0,i}}{k_{0,s}}$, due to the continuity condition at $F = F_{s-i}$. Thus, the slip-ideal model can be written as either

$$k_{\text{off},s-i}(F(t)) = \begin{cases} k_{0,s} e^{\frac{F(t)}{F_s}} & F < F_{s-i} \\ k_{0,s} e^{\frac{F_{s-i}}{F_s}} & F \geq F_{s-i} \end{cases} \quad (10b)$$

or

$$k_{\text{off},s-i}(F(t)) = \begin{cases} k_{0,s}e^{-\frac{F(t)}{F_s}} & F < \alpha F_s \\ k_{0,s}e^{\alpha} & F \geq \alpha F_s \end{cases} \quad (10c)$$

Unfortunately, the piecewise nature of Eq. (10) does not lend itself well to further mathematical analysis. However, there are multiple approaches to approximating slip-ideal bonds, which enable further analysis and ultimately fitting data to Eq. (2). These approaches include a Michaelis–Menten or Langmuir absorption-like function (Fig. 2b)³³, a sigmoidal model approximation (Fig. 2c), and a rational interpolation^{35,36} approach (Fig. 2c) that uses the RationalInterpolation function in Mathematica³⁷, for example. See the Supplementary Information for a more detailed discussion on these approximations of slip-ideal bonds.

Catch bonds. The unbinding constant of the catch bond, $k_{\text{off},c}$, decreases exponentially with force per Bell’s model¹⁷,

$$k_{\text{off},c}(F(t)) = k_{0,c}e^{-\frac{F(t)}{F_c}} \quad (11)$$

So, for a constant loading and n_0 observable events, Eq. (2) becomes

$$n(t) = Ne^{-\frac{F_c k_{0,c}}{f} \left(1 - e^{-\frac{ft}{F_c}}\right)} \quad (12a)$$

or

$$n(t) = n_0 e^{-\frac{F_c k_{0,c}}{f} \left(e^{-\frac{ft_0}{F_c}} - e^{-\frac{ft}{F_c}}\right)} \quad (12b)$$

However, this is a relatively limited model because it models the unbinding rate constant as going to zero as F goes to infinity. Equation (11) suggests that a catch bond will never break under an arbitrarily high load, which is non-physical. Therefore, Eq. (11) is only valid for low force. All known catch-bonds invariably transform into slip or ideal bonds as the forces increase beyond a critical value^{38,39}. To capture the high-loading case, one can model all catch bonds as catch-slip or catch-ideal bonds.

Catch-ideal bonds. A simple, theoretically appealing way to correct for the physical limitation of the catch bond is with a catch-ideal bond. A catch-ideal bond can be modeled as a bond that behaves like a catch bond under low loading and an ideal bond after the force crosses the catch-ideal transition force, F_{c-i} . The unbinding constant of the catch-ideal bond, $k_{\text{off},c-i}$ (Fig. 2e), is

$$k_{\text{off},c-i}(F(t)) = \begin{cases} k_{0,c}e^{-\frac{F(t)}{F_c}} & F < F_{c-i} \\ k_{0,c}e^{-\frac{F_{c-i}}{F_c}} & F \geq F_{c-i} \end{cases} \quad (13a)$$

or

$$k_{\text{off},c-i}(F(t)) = \begin{cases} k_{0,c}e^{-\frac{F(t)}{F_c}} & F < F_{c-i} \\ k_{0,i} & F \geq F_{c-i} \end{cases} \quad (13b)$$

where only three of the four parameters are independent: $k_{0,i} = k_{0,c}e^{-\frac{F_{c-i}}{F_c}}$ or $F_{c-i} = F_c \ln \frac{k_{0,c}}{k_{0,i}}$, due to the continuity condition at $F = F_{c-i}$.

We can approximate Eq. (13) with a sigmoidal function,

$$k_{\text{off},c-i}(F(t)) = (k_{0,c} - k_{0,i})e^{-\frac{F(t)}{\left(1 - \left(\frac{k_{0,i}}{k_{0,c}}\right)^q\right)F_c}} + k_{0,i} \quad (14)$$

At zero force, the sigmoidal approximation behaves like a catch bond, $k_{\text{off},c-i}(0) = k_{0,c}$, and $k_{\text{off},c-i}(F \rightarrow \infty) \rightarrow k_{0,i}$ as force goes to infinity. Equation (14) shares the same initial slope, $\frac{\partial k_{\text{off},c-i}}{\partial F} (0) = -\frac{k_{0,c}}{F_c}$, with Eq. (13) if $q = 1$, and it represents a simpler approximation, that $k_{\text{off},c-i}(F(t)) = (k_{0,c} - k_{0,i})e^{-\frac{F(t)}{F_c}} + k_{0,i}$, for q goes to infinity (Fig. 2e). The best fit of Eq. (14) to the piecewise function (Eq. (13)), found with a least-squares regression, Mathematica) occurs when $q = 0.60$ (Fig. 2e). For constant loading rate, Eq. (2) becomes

$$n(t) = Ne^{-\left(\frac{\left(1 - \left(\frac{k_{0,i}}{k_{0,c}}\right)^q\right)F_c (k_{0,c} - k_{0,i})}{f} \left(1 - e^{-\frac{ft}{\left(1 - \left(\frac{k_{0,i}}{k_{0,c}}\right)^q\right)F_c}}\right) - k_{0,i}t\right)} \quad (15a)$$

or

$$n(t) = n_0 e^{\left(\frac{\left(1 - \left(\frac{k_{0,i}}{k_{0,c}}\right)^q\right) F_c (k_{0,c} - k_{0,i})}{f} \left(e^{-\left(\frac{ft_0}{k_{0,c}}\right)^q} F_c - e^{-\left(\frac{ft}{k_{0,c}}\right)^q} F_c \right) - k_{0,i}(t-t_0) \right)} \quad (15b)$$

Catch-slip bonds. While the catch-ideal bond is appealing, there is a stronger theoretical basis of^{38,40} and experimental evidence for⁴¹ catch-slip bonds. The conceptual model of a catch-slip bond suggests a transition from catch bond to slip bond behavior when the force exceeds a critical catch-slip transition value, F_{c-s} . A five-parameter piecewise function can mathematically model catch-slip bonds (Fig. 2f),

$$k_{\text{off},c-s}(F(t)) = \begin{cases} k_{0,c} e^{-\frac{F}{F_c}} & F \leq F_{c-s} \\ k_{0,s} e^{\frac{F}{F_s}} & F > F_{c-s} \end{cases}, \quad (16)$$

where only four parameters are independent because $k_{0,c} e^{-\frac{F_{c-s}}{F_c}} = k_{0,s} e^{\frac{F_{c-s}}{F_s}}$, or equivalently $F_{c-s} = \frac{F_c F_s}{F_c + F_s} \ln\left(\frac{k_{0,c}}{k_{0,s}}\right)$, due to the continuity condition at $F = F_{c-s}$.

Catch-slip bonds have been modeled as dissociating through one of two independent pathways: the catch bond pathway at relatively low force and short times, and the slip bond pathway at relatively high force and long times¹⁰. The analytical expression for this model is

$$k_{\text{off},c-s}(F(t)) = k_{0,c} e^{-\frac{F}{F_c}} + k_{0,s} e^{\frac{F}{F_s}}, \quad (17)$$

provided $\frac{k_{0,c}}{F_c} < \frac{k_{0,s}}{F_s}$ (Fig. 2f). In this case, the catch-slip transition force, $F_{c-s} = \frac{F_c F_s}{F_c + F_s} \ln\left(\frac{k_{0,c} F_s}{k_{0,s} F_c}\right)$, occurs when the first derivative of Eq. (17) with respect to force is zero. For constant loading rate, Eq. (2) becomes

$$n(t) = N e^{-\left(\frac{F_s k_{0,s} \left(e^{\frac{ft}{F_s}} - 1 \right) + F_c k_{0,c} \left(1 - e^{-\frac{ft}{F_c}} \right)}{f} \right)} \quad (18a)$$

or

$$n(t) = n_0 e^{-\left(\frac{F_s k_{0,s} \left(e^{\frac{ft}{F_s} - \frac{ft_0}{F_s}} \right) + F_c k_{0,c} \left(e^{-\frac{ft_0}{F_c} - \frac{ft}{F_c}} \right)}{f} \right)} \quad (18b)$$

Force-jump assays. Force jump^{28,42–44} and ultrafast force clamp⁴⁵ assays have recently become popular ways to use the optical tweezer. When these assays are used to probe the biophysical properties of biomolecular bonds, the applied force quickly increases to a constant value, F_j , and held constant to study the detachment of bonds at a constant force. We consider the jumping process to have a large but finite force ramp, f_j , then, independent of bond type, we evaluate Eq. (2) in a piecewise manner,

$$n(t) = N e^{-\left(\int_0^{t_j} k_{\text{off}}(f_j t') dt' + \int_{t_j}^t k_{\text{off}}(F_j) dt' \right)} \quad (19a)$$

where the jump time, $t_j = \frac{F_j}{f_j}$, is the time required to reach the constant force. If we solve Eq. (19a) for $t = t_j$, we find that the number of bonds that survive the jump is $N_j = N e^{-\int_0^{t_j} k_{\text{off}}(f_j t') dt'}$, and thus Eq. (2) becomes

$$n(t) = N_j e^{-k_{\text{off}}(F_j)(t-t_j)} \quad (19b)$$

for $t > t_j$. Most force-jump assays are designed to minimize N_j , and for the case where $N_j < N - n_0$ (less than the number of events lost in the noise), Eq. (19b) is equivalent to a constant force dissociation assay. If $N_j > N - n_0$, one must extend the analysis we presented above to account for bonds that dissociated during the rapid ramp and the constant force experimental regimes, which one can do by knowing the applied constant force and how many bonds dissociated in the constant force regime. In either case, to characterize the biophysical properties of the bond, one would have to perform the experiment at many values of the applied constant force, F_j , greatly increasing the amount of data one must collect as compared to a force-ramp assay.

Simulations

We stochastically simulated the unbinding of non-covalent, biomolecular bonds in MATLAB⁴⁶ using the Gillespie algorithm⁴⁷. We considered a system with N independently attached bonds at time $t = 0$ and applied a constantly increasing force (with constant loading rate f) to each bond. We simulated the time at which each bond, $i = 1 \rightarrow N$, broke, $t_i = t_{i-1} + \tau_i$, where

$$\tau_i = -\frac{\ln(r)}{n(t_i) k_{\text{off}}(F(t_i))} \quad (20)$$

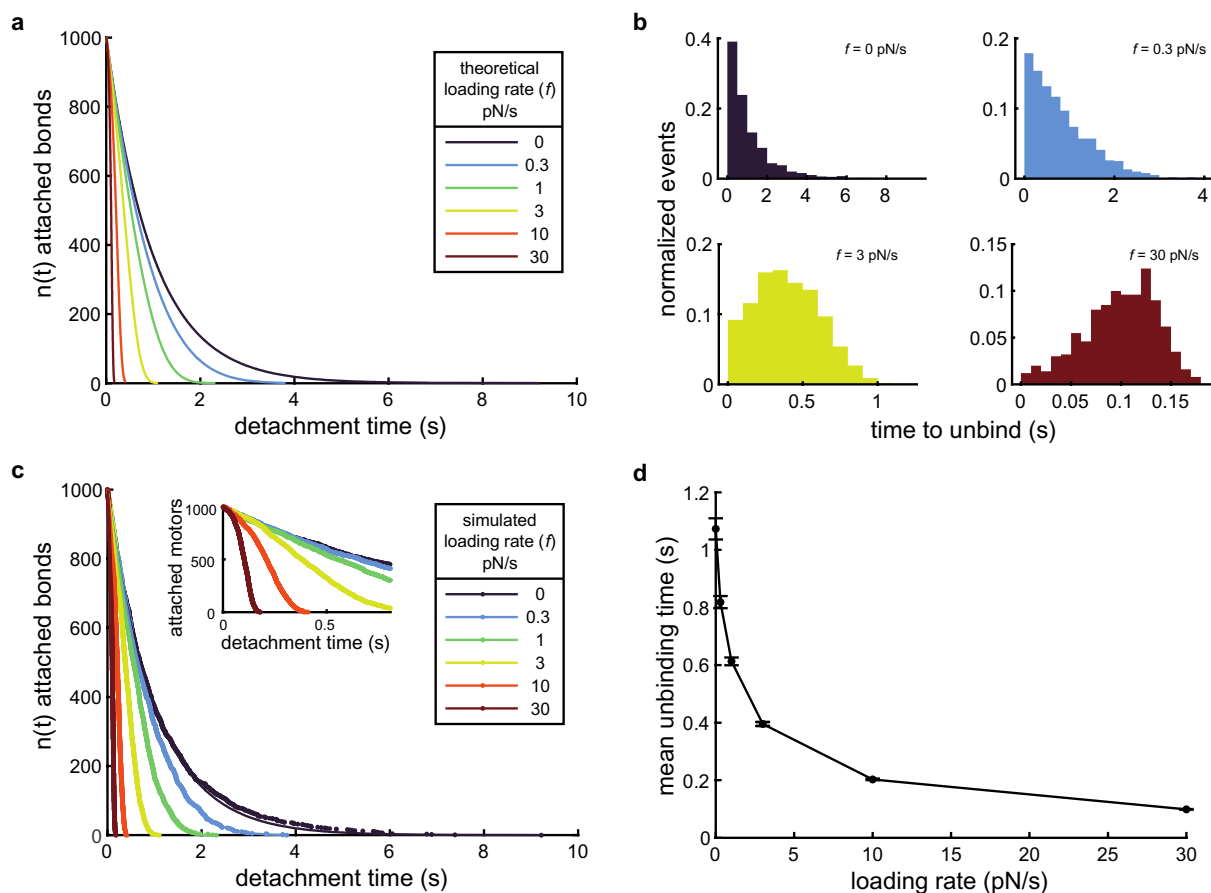


Figure 3. Calculating the force-dependent unbinding rate for slip bonds. **(a)** $n(t) = Ne^{-k_{0,s}t}$ plotted for no loading (dark purple line) and Eq. (5) plotted for various loading rates (colored lines) with $N = 1000$ slip bonds that have an unloaded unbinding rate $k_{0,s} = 1 \text{ s}^{-1}$ and force sensitivity $F_s = 1 \text{ pN}$. **(b)** Histograms of the time to unbind from a typical, $N = 1000$, slip bond simulation with parameters as in panel (a) for various loading rates, as indicated. **(c)** Number of bound slip bonds as a function of time from example simulations at various loading rates, as indicated. Inset shows detail highlighting the characteristic shape of $n(t)$ for higher loading rates (3 pN/s yellow, 10 pN/s orange, and 30 pN/s dark red). The data (dots) were fitted to $n(t) = Ne^{-k_{0,s}t}$ for $f = 0$ (dark purple line) and Eq. (5) for the others (lines). In both cases, see Table S2 for the fit parameters. The same example simulation data were used as in panel (b), where applicable. **(d)** Mean unbinding time of 50 simulations, with $N = 1000$ slip bonds each, as a function of loading rate. The error bars represent s.e.m.

per standard implementation of the Gillespie algorithm⁴⁸, r is a random number between 0 and 1 sampled from a uniform distribution, $n(t_i) = N - i$ is the number of bonds that remain attached after time t_i , and $k_{\text{off}}(F(t_i))$ is the force-dependent unbinding constant.

Results and discussion

We demonstrate the benefits of fitting single-molecule unbinding data to the cumulative distribution function-like $n(t)$ over more traditional histogram analysis using simulated data. We do so, rather than using example experimental data, to demonstrate the power of this analysis on datasets for which we know the underlying biophysical nature of the bonds because we set them in the simulations. We use slip bonds and catch-slip bonds as examples (for brevity) because they are commonly reported bond types in the literature. However, the analysis could be easily extended to the other bond types and approximations of their functional forms, as discussed above and the Supplementary Information.

Slip bonds. We simulated $N = 1000$ slip bonds with unloaded unbinding rate $k_{0,s} = 1 \text{ s}^{-1}$ and force sensitivity $F_s = 1 \text{ pN}$ subjected to no loading ($k_{\text{off},s}(F = 0) = k_{0,s}$ per Eq. (3) and $n(t) = Ne^{-k_{0,s}t}$, Fig. 3a) and with linearly increasing loads ($k_{\text{off},s}(F = ft)$ per Eq. (4) and $n(t)$ per Eq. (5), Fig. 3a). By comparing histograms of the time to detach for 1000 simulated bonds (Fig. 3b), we found that the time to detachment distribution was a strong function of loading rate. With no external load ($F = 0$, Fig. 3b, upper left), the histogram took the form of exponential decay, as expected for a single kinetic process. However, the characteristic form of the histogram became increasing Gaussian-like (though not strictly Gaussian) as the loading rate, f , increased (Fig. 3b).

We also plotted the force-free and force-dependent dissociation of simulated slip bonds (same data as Fig. 3b) as a function of their time to dissociate ($n(t)$). We fit these data to $n(t) = Ne^{-k_{0,s}t}$ and Eq. (5) (Fig. 3c, Table S2,

Loading rate (pN/s)	$k_{0,s}$ (s^{-1}) (Fit \pm s.e.m.)	P value	F_s (pN) (Fit \pm s.e.m.)	P value
Simulation parameter	1	–	1	–
0	1.009 \pm 0.005	0.06	–	–
0.3	0.990 \pm 0.008	0.21	1.019 \pm 0.038	0.62
1	0.995 \pm 0.009	0.58	0.998 \pm 0.015	0.88
3	1.018 \pm 0.008	0.06	1.010 \pm 0.008	0.25
10	0.992 \pm 0.012	0.48	0.997 \pm 0.006	0.67
30	0.996 \pm 0.016	0.81	1.002 \pm 0.006	0.69

Table 1. Mean fit parameters from simulated slip bond dissociation data sets. Reported values represent the mean \pm s.e.m. of the fit parameters for 50 sets of $N = 1000$ simulated slip bond dissociations under the increasing load rate, as indicated. In all cases, P values are calculated for two-tailed t-tests.

and Supplementary Information for details), respectively. We repeated the simulations 50 times and calculated the mean fitting parameters for each loading rate (Table 1). We found that the means of the fit parameters, $k_{0,s}$ and F_0 , were not significantly different from the corresponding parameters used in the simulations (P values > 0.05 in all cases, Table 1, two-tailed t-tests). Thus, our cumulative distribution function-like analysis uniquely and accurately determined the underlying biophysical parameters associated with slip bonds at each loading rate, suggesting one only needs to collect one such data set to characterize a slip bond.

We also calculated the mean detachment time for each force-ramp loading rate condition (Fig. 3d). In the unloaded case, the mean unbinding time was 1.073 s for the example data in Fig. 3b, which was similar to but not a particularly great predictor of (7.3% error) the expected value of $\frac{1}{k_{0,s}}$ (1 s, for this simulation) for a first-order kinetic process (Supporting Information). However, when extending this analysis to the force-dependent unbinding properties, we found that the mean of the detachment time decreased with increasing loading rate (Fig. 3d). Therefore, the underlying biophysical parameters of the bond are inaccessible to histogram analysis without explicitly accounting for the loading rate, and even then, it requires collecting large data sets at multiple loading rates (Supplementary Information for more details).

The effect of experimental noise on slip bonds. In an experiment (e.g., Fig. 1a), it is impossible to distinguish single-molecule dissociation data for short times from the noise associated with the experiments. The noise “hides” detachment events if the detected data are smaller than four to five times the standard deviation of the noise. Selecting a detection threshold as high as five times the standard deviation is necessary to avoid misinterpreting the noise as a molecular unbinding event because the data collection rate necessary for high temporal resolution necessitates capturing many data points. For example, one would expect to misinterpret noise as a binding event 380 times with a 4σ threshold and 3.4 times with a 5σ threshold, on average, for 5 min of data collection at a 20 kHz sampling rate (6,000,000 data points). Depending on the total number of events within the measurement time, but frequently of order 10^2 – 10^3 events, hundreds of false-positive events could lead to a significant misinterpretation of the results. Given a loading rate, this detection threshold sets and effective minimum time for events, a detection threshold of t_0 , as described above.

We applied a detection threshold of $t_0 = 50$ ms to the example simulated data in Fig. 3b, and we found that the mean unbinding time in the unloaded case increased to 1.130 s from 1.073 s with $t_0 = 0$ ms (P value = 0.28, two-tailed t-test). However, in the case of $f = 30$ pN/s, we found that the mean unbinding time increased to 0.1075 s from 0.0991 s with $t_0 = 0$ ms (P value < 0.0001 , two-tailed t-test). These results highlight the conclusion that the underlying biophysical parameters of the bond are inaccessible in histogram analysis without specifically accounting for the loading rate and the detection limit (Supplementary Information for more details).

We further probed the effect of the detection limit by discarding all data from our 50 simulations (same data as used in Table 1) with unbinding time $t < t_0 = 50$ ms. We found that 50 to 110 data points of the $N = 1000$ were “hidden,” on average, by the detection limit ($N - n_0$, Table 2), representing the shortest 5 to 11% of the events in the simulated data sets. The biased nature of the data loss (short events), and the strong effect of loading rate on the extent to which the data is lost (Table 2) makes estimating the number of “hidden” datapoints to from an experimental data set difficult. This data loss significantly affects any quantitative analysis of unbinding time histograms, as described above and detailed in the Supplementary Information.

However, we found that the situation was much improved when we fit these data to $n(t) = n_0 e^{-k_{0,s}(t-t_0)}$ and Eq. (9) using the number of “detected” unbinding events in each simulation, n_0 , f , and $t_0 = 50$ ms as fixed parameters. We calculated the mean of the 50 sets of fitting parameters for each loading rate (Table 2). We found that the means were not significantly different from the parameters used in the simulations, i.e., $k_{0,s} = 1$ s $^{-1}$ and $F_s = 1$ pN (P values > 0.05 in all cases, Table 2, two-tailed t-tests), and that none of the mean fitting parameters were significantly different from the fitting parameters found using all the data (P values > 0.05 in all cases, comparing data in Table 1 and Table 2, two-tailed t-tests). Thus, despite the “hidden” data, we showed that our cumulative distribution function-like analysis unambiguously recovers the physical parameters of the slip bonds.

Catch-slip bonds. We also simulated $N = 1000$ catch-slip bonds with an unloaded unbinding rate of $k_{0,c} = 1$ s $^{-1}$, catch bond force sensitivity $F_c = 1$ pN, slip bond unloaded unbinding rate $k_{0,s} = 0.05$ s $^{-1}$, and slip bond force sensitivity $F_s = 1$ pN (the same parameters used in Fig. 2f, these equate to $F_{c-s} = 1.5$ pN) subjected to linearly increasing loads ($k_{\text{off},c-s}(F = ft)$ per Eq. (16) and $n(t)$ per Eq. (18), Fig. 4a), as well as with no loading

Loading rate (pN/s)	n_0 (Mean \pm s.e.m.)	$k_{0,s}$ (s^{-1}) (Fit \pm s.e.m.)	P value	F_s (pN) (Fit \pm s.e.m.)	P value
Simulation parameter	1000	1	–	1	–
0	950.3 ± 1.1	1.008 ± 0.005	0.11	–	–
0.3	951.2 ± 1.0	0.990 ± 0.009	0.24	1.030 ± 0.044	0.49
1	950.6 ± 1.0	0.997 ± 0.010	0.79	1.003 ± 0.016	0.86
3	946.2 ± 1.1	1.013 ± 0.010	0.20	1.008 ± 0.010	0.41
10	937.1 ± 1.1	0.987 ± 0.014	0.34	0.995 ± 0.007	0.49
30	890.5 ± 1.3	0.984 ± 0.022	0.48	0.997 ± 0.008	0.74

Table 2. Mean fit parameters from simulated slip bond dissociation data sets where short events have been removed. Reported values represent the mean \pm s.e.m. of the fit parameters for the same 50 sets of simulated slip bond dissociation data as in Table 1, but where short events corresponding to those that are indistinguishable from experimental noise have been removed. In all cases, P values are calculated for two-tailed t-tests.

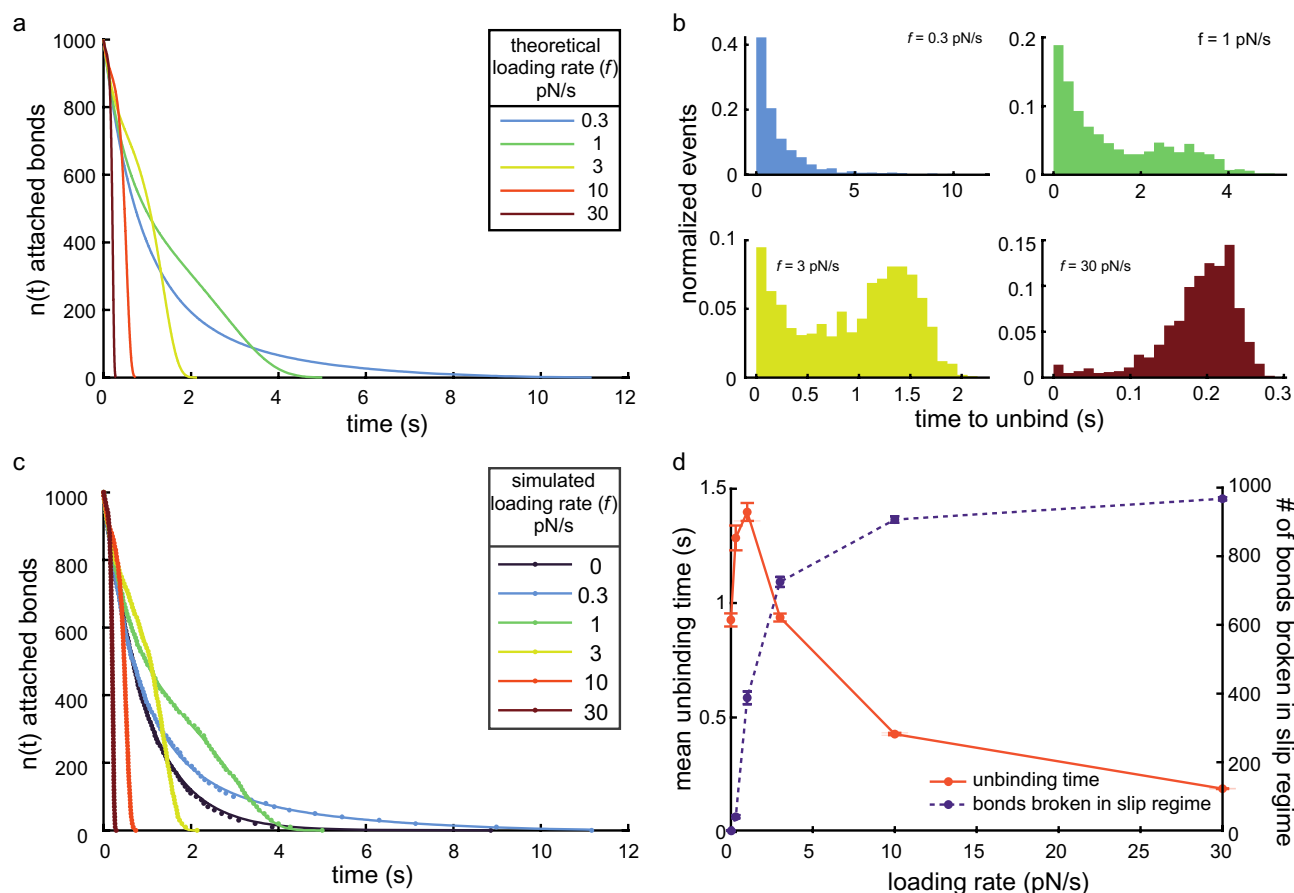


Figure 4. Calculating the force-dependent unbinding rate for catch-slip bonds. (a) Eq. (18a) plotted for various loading rates (colored lines) with $N = 1000$ slip bonds an unloaded unbinding rate of $k_{0,c} = 1 \text{ s}^{-1}$, catch bond force sensitivity of $F_c = 1 \text{ pN}$, slip bond unbinding rate of $k_{0,s} = 0.05 \text{ s}^{-1}$, and slip bond force sensitivity of $F_s = 1 \text{ pN}$, as in Fig. 2f. (b) Histograms of the time to unbind from a typical $N = 1000$ slip bond simulation with parameters as in (a) for various loading rates, as indicated. (c) Number of bound catch-slip bonds as a function of time for example simulations at various loading rates, as indicated. The data (dots) were fit to $n(t) = Ne^{-k_{0,c}t}$ for $f = 0$ (dark purple line) and Eq. (18a) for the others (lines). The equations were well-fit to the data in all of the example cases shown here, see Table S3 for the fit parameters and Supplementary Information for more detail. The same example simulation data were used as in panel (b), where applicable. (d) Mean unbinding time (orange solid line, left axis) and mean number of bonds broken in the slip bond regime (purple dashed line, right axis) of 50 simulations, with $N = 1000$ catch-slip bonds each, as a function of loading rate. The error bars represent the s.e.m. on both data sets.

Loading rate (pN/s)	Significant fits	$k_{0,c}$ (s^{-1}) (Mean \pm s.e.m.)	P value	F_c (pN) (Mean \pm s.e.m.)	P value	$k_{0,s}$ (s^{-1}) (Mean \pm s.e.m.)	P value	F_s (pN) (Mean \pm s.e.m.)	P value
Simulation parameter	50	1	–	1	–	0.05	–	1	–
0	50	1.0478 \pm 0.0054	0.69	–	–	–	–	–	–
0.3	22	1.0058 \pm 0.0171	0.74	1.1698 \pm 0.0698	0.02	0.0360 \pm 0.0160	0.39	0.6043 \pm 0.1441	0.01
1	50	1.0115 \pm 0.0109	0.30	0.9826 \pm 0.0342	0.61	0.0589 \pm 0.0048	0.07	1.0341 \pm 0.0304	0.27
3	50	1.0146 \pm 0.0145	0.32	1.0467 \pm 0.0295	0.12	0.0485 \pm 0.0017	0.38	0.9878 \pm 0.0093	0.20
10	47	1.0965 \pm 0.0326	0.005	1.0120 \pm 0.0547	0.82	0.0496 \pm 0.0016	0.98	0.9952 \pm 0.0065	0.46
30	40	1.3684 \pm 0.0795	< 0.0001	0.8083 \pm 0.0924	.04	0.0502 \pm 0.0021	0.92	0.9974 \pm 0.0070	0.71

Table 3. Mean fit parameters from simulated catch-slip bond dissociation data sets. Reported values represent the mean \pm s.e.m. of the fit parameters for the sets of $N = 1000$ simulated catch-slip bond dissociations under the increasing load rate for which the fits were significant. The number of significant fits is indicated. In all cases, P values are calculated for two-tailed t-tests. * $k_{\text{off},c-s}(F = 0) = k_{0,c} + k_{0,s} = 1.05$ per Eq. (17) for the parameters used in the simulation.

($k_{\text{off},c-s}(F = 0) = k_{0,c}$ per Eq. (16) and $n(t) = Ne^{-k_{0,c}t}$, equivalent to the unloaded slip bond case, Fig. 3a, dark purple). We found that the nature of the time to detach distribution histograms was a strong function of loading rate. Low external loading rates ($f = 0.3$ pN/s, Fig. 4b, upper left) exhibited a nearly exponential distribution of unbinding times, like the other bond types we have discussed, and high external loading rates ($f = 30$ pN/s, Fig. 4b, lower right) corresponded to a large Gaussian-like distribution of unbinding events at longer times. It is in the intermediate loading rate regime that two separate peaks, coming from the separate, significant contributions from the catch bond (short events) and slip bond (long events) behaviors, respectively, emerge (Fig. 4b, upper right and lower left).

We also plotted the force-free and force-dependent dissociation of simulated slip bonds (same data as Fig. 4b) as a function of their time to dissociate ($n(t)$). We fit these data to $n(t) = Ne^{-k_{0,s}t}$ and Eq. (18a) (Fig. 4c, Table S3, and Supplementary Information for details), respectively. As we did with slip bonds, we input the values for N and f as fixed parameters in the fit and repeated the simulations 50 times. Unlike the case of slip bonds, we found that non-linear least squares regression was unable to uniquely determine fitting parameters in multiple of the simulated data sets at lower and higher loading rates (Supplementary Information). Of the 50 simulations, we found that only 22 of the simulated data sets were well-fit by Eq. (18a) for low loading rate (0.3 pN/s) and 40 of the simulated data sets were well-fit by Eq. (18a) for high loading rate (30 pN/s).

We suspected that the errors in the fits were due to an “overfitting” of the data, that is, the number of data points become too few in either the catch bond (short events) or slip bond (long events) regimes, so the model effectively has more parameters than can be justified by the data. Overfitting makes the model insensitive to the data, and the fit values become unreasonably small or large. To investigate this hypothesis, we determined whether the force at unbinding was above or below the catch-slip transition force, F_{c-s} , for each unbinding event to classify whether the bond dissociated in the catch ($F < F_{c-s}$) or slip ($F > F_{c-s}$) regime. We plotted the mean number of bonds dissociating in the slip regime for the 50 simulations with $N = 1000$ total bonds (Fig. 4d, purple dashed line). We found that most of the bonds dissociated in the catch bond regime (Fig. 4d, purple dashed line) when the loading rate was low, corresponding to an exponential-like distribution of unbinding events (Fig. 4b, upper left). At high loading rates, the fraction of bonds that dissociated in the slip force regime was high (Fig. 4d, purple dashed line), corresponding to a large Gaussian-like distribution at relatively longer times (Fig. 4b, lower right) and similar to slip bonds (Fig. 3b, lower right). Together, these data suggest that the slip bond parameters have little effect on the unbinding behaviors at low loading rates and that the catch bond parameters have little effect on the unbind behaviors at high loading rates. Thus, attempting to fit Eq. (18a), which contains both the slip and catch bond-related parameters, is less effective at low or high loading rates.

Moreover, even when the low and high loading rate data are well-fit by Eq. (18a), i.e., the non-linear least squares regression was able to uniquely determine fitting parameters, we found that the standard errors of those fits tend to be significantly larger than for intermediate loading rates (Tables 3 and S3, and Supplementary Information for more details). Therefore, these results suggest that one must use intermediate loading rates, i.e., loading rates for which a significant number of bonds dissociate in the catch and slip regimes (Fig. 4d, purple dashed line), to determine the biophysical properties of catch-slip bonds, which is consistent with previously reported results^{12,28}. The loading rate for which 50% of the bonds dissociates at the catch and slip bonds regime is given by

$$f'_{c-s} = \frac{F_c k_{0,c} \left(1 - e^{-\frac{F_c}{F_c}}\right) - F_s k_{0,s} \left(1 - e^{-\frac{F_s}{F_s}}\right)}{\ln(2)}. \quad (21)$$

$f'_{c-s} = 1.37$ pN/s for the parameters used above and in Fig. 4. Equation 21 is only valid for catch-slip bonds; however, a similar analysis can be performed for any bond type.

We also calculated the mean detachment time for each force-ramp loading rate condition (Fig. 4d, orange solid line). We found that the mean detachment time increased for faster loading rates while the dissociations were dominated by the catch-bond behavior (Fig. 4d, purple dashed line). However, this trend reversed at an intermediate loading rate and the mean detachment time decreased with increasing loading rate (Fig. 4d, orange

Loading rate (pN/s)	Significant fits	n_0 (Mean \pm s.e.m.)	$k_{0,c}$ (s ⁻¹) (Mean \pm s.e.m.)	<i>P</i> value	F_c (pN) (Mean \pm s.e.m.)	<i>P</i> value	$k_{0,s}$ (s ⁻¹) (Mean \pm s.e.m.)	<i>P</i> value	F_s (pN) (Mean \pm s.e.m.)	<i>P</i> value
Simulation parameter	50		1	–	1	–	0.05	–	1	–
0	50	949.4 \pm 1.1	1.0484* \pm 0.0053	0.76	–	–	–	–	–	–
0.3	24	948.4 \pm 0.8	0.9956 \pm 0.0164	0.79	1.1764 \pm 0.0678	0.02	0.0391 \pm 0.0150	0.47	0.6217 \pm 0.1397	0.01
1	50	949.3 \pm 1.0	1.0149 \pm 0.0128	0.25	0.9944 \pm 0.0416	0.89	0.0594 \pm 0.0050	0.06	1.0348 \pm 0.0317	0.28
3	50	950.6 \pm 0.7	0.9972 \pm 0.0214	0.90	1.1124 \pm 0.0449	0.02	0.0472 \pm 0.0018	0.13	0.9812 \pm 0.0095	0.05
10	33	957.0 \pm 0.9	1.3098 \pm 0.1197	0.01	1.1293 \pm 0.1145	0.27	0.0482 \pm 0.0017	0.30	0.9897 \pm 0.0075	0.18
30	5	967.7 \pm 0.6	0.9693 \pm 0.3377	0.93	0.7971 \pm 0.2214	0.41	0.0541 \pm 0.0049	0.45	1.0131 \pm 0.0159	0.46

Table 4. Mean fit parameters from simulated catch-slip bond dissociation data sets where short events have been removed. Reported values represent the mean \pm s.e.m. of the fit parameters for the same 50 sets of simulated slip bond dissociation data for which the fits were significant, as in Table 2, but where short events corresponding to those that are indistinguishable from experimental noise have been removed. The number of significant fits is indicated. In all cases, *P* values are calculated for two-tailed t-tests.

* $k_{\text{off},c-s}(F = 0) = k_{0,c} + k_{0,s} = 1.05$ per Eq. (17) for the parameters used in the simulation.

solid line) as more the dissociations were dominated by the slip-bond behavior (Fig. 4d, *purple dashed line*). We had found that determining the underlying biophysical parameters of slip bonds from characterizations of the mean unbinding time and associated histograms requires collecting large data sets at multiple loading rates (Supplementary Information for more details). However, we found that, to the best of our knowledge, an equivalent analysis did not yield analytical solutions, even with special functions, from which we could calculate the underlying biophysical parameters of catch-slip bonds using the mean unbinding time and associated histograms.

Together, this analysis and these data highlight the importance of performing single-molecule experiments at optimized experimental conditions, i.e., ones that enable characterization of all the physics associated with catch-slip bonds, and the utility of our cumulative distribution-like analysis.

Effect of experimental noise on catch-slip bonds. As discussed above, noise in force-spectroscopy data can hide dissociations that occur at short times. To investigate the role of experimental noise on the analysis of catch-slip bonds, we excluded simulated dissociation events from our 50 simulations (same data as used in Table 3) with unbinding time $t < t_0 = 50$ ms. We fit $n(t)$ with Eq. (18b) to calculate the corresponding bond parameters (Table 4). We found that non-linear least squares regression uniquely determined fitting parameters in fewer of the simulated data sets, particularly at higher loading rates, than when not accounting for experimental noise (Supporting Information). Of the 50 simulations, we found that only 24 of the $f = 0.3$ pN/s, 33 of the $f = 10$ pN/s, and 5 of the $f = 30$ pN/s simulated data sets were well-fit by Eq. (18b) (Table 4).

As we observed for the simulated data without accounting for the effect of experimental noise (Table 3), the cumulative distribution function-like analysis technique was able to resolve the catch-bond fitting parameters reasonably well (despite a 17%, *P* value = 0.02 two-tailed t-test, error in resolving the force sensitivity of the catch bond) with low s.e.m. of the fits in low loading rate simulations, and the slip-bond fitting parameters (despite a low number of well-fit data sets) in the high loading rate simulation (Table 4). Additionally, as we observed for the simulated data without accounting for experimental noise (Table 3), catch-bond fitting parameters were not well resolved at high loading rate simulations, and slip-bond fitting parameters were not well resolved at low loading rates (Table 4). Like we found with slip bonds, none of the fit parameters differed significantly from those found when accounting for the complete simulated data set (*P* values > 0.05, two-sample two-tailed t-tests, Tables 3 and 4), again highlighting the benefit of our method when analyzing noisy experimental data.

These data again serve to highlight the effectiveness of the cumulative distribution-like analysis to resolve the biophysical parameters associated with catch-slip bonds, even when experimental noise hides short events. However, the reduction in the number of well-fit data sets, and the increased sensitivity of the catch bond parameters to the loading rate when short events are hidden by noise, does strongly suggest that loading rates must be chosen carefully, particularly for catch-slip bonds with relatively low catch-slip transition force, F_{c-s} .

Conclusion

We presented an analytically derived cumulative distribution-like function of unbinding events ($n(t)$) for various biological macromolecular bond types when subject to force. We showed how an $n(t)$, cumulative distribution function-like, based approach can be used to analyze force-dependent dissociation force spectroscopy data. We demonstrated the benefits and limitations of the technique using stochastic simulations (Gillespie algorithm) of slip and catch-slip bonds. The approach can determine the detachment rate and force sensitivity of biological macromolecular bonds from force spectroscopy experiments by explicitly accounting for loading rate more efficiently than histogram-based analyses. This analysis approach requires fewer, smaller data sets than alternative approaches. Additionally, the approach returns similar (not statistically different) results when short events are hidden by noisy data. We suggest that this approach provides an improved systematic and quantitative method to distinguishing various bond types and characterizing their underlying biophysical properties.

We also analyzed the effect of using a range of loading rates to probe the force-dependent unbinding of biological macromolecules. Our simulated data suggests that this analysis of slip-bonds is largely insensitive to

loading rate. However, care must be taken to ensure a significant fraction of the bonds dissociate in both the catch- and slip-bond force regimes, when the bond is a catch-slip bond. Thus, if an experiment is being done on a bond of unknown type, multiple loading rates are necessary to ensure all possible molecular dissociation pathways are sufficiently sampled in the experiments to resolve their underlying biophysical parameters.

We recommend that users implement the following tips when using our analysis approach to analyze the force-dependent dissociation of biomolecular bonds in optical tweezer force ramp experiments. First, our stochastically simulated force-dependent unbinding data demonstrated the importance of selecting an appropriate loading rate. Since the underlying biophysical parameters, or type, of a bond are presumably unknown at the time of the experiment, our simulations suggest one should first use a range of test loading rates over multiple orders of magnitude to initially characterize the bond type. Once the bond type has been identified, one should probe at an appropriate rate for the characteristic timescale of the dissociation. Our results suggest that using a loading rate that causes 50% of the bonds to dissociate in the catch and slip bonds regimes, f'_{c-s} per Eq. (21), for catch-slip bonds, for example. Additionally, our results show that despite being better than a histogram approach, the confidence interval of the force-dependent dissociation parameters of a bond determined using our cumulative distribution-like analysis from a single dataset may not include the actual value of the underlying bond's properties. However, our results suggest that one can mitigate this issue by averaging the fitting parameters from multiple force-dependent dissociation datasets. Finally, our results and analyses provide a means to account for experimental noise, not the least of which is thermal in nature, and the unbinding events that will invariably be missed when performing force-dependent dissociation assays with optical tweezers. We suggest that one can implement t_0 , a timescale representing the shortest observable event in a linear force ramp experiment, without any loss of sensitivity.

In summary, our approach provides a framework for an improved analysis of force-dependent biological macromolecular dissociation force spectroscopy data. It explicitly accounts for the loading rate, which may be complicated by optical tweezer trap stiffness and biological macromolecular stiffness, to distinguish between and fully characterize the biophysical properties of protein–protein and protein–ligand bonds.

Received: 23 September 2021; Accepted: 8 December 2021

Published online: 07 January 2022

References

1. Thomas, W. E., Vogel, V. & Sokurenko, E. Biophysics of catch bonds. *Annu. Rev. Biophys.* **37**, 399–416 (2008).
2. Howard, J. *Mechanics of Motor Proteins and the Cytoskeleton* (Sinauer Associates, 2001).
3. Marshall, B. T. *et al.* Direct observation of catch bonds involving cell-adhesion molecules. *Nature* **423**, 190–193 (2003).
4. Priest, A. V., Shafraz, O. & Sivasankar, S. Biophysical basis of cadherin mediated cell–cell adhesion. *Exp. Cell Res.* **358**, 10–13 (2017).
5. Rakshit, S. & Sivasankar, S. Biomechanics of cell adhesion: how force regulates the lifetime of adhesive bonds at the single molecule level. *Phys. Chem. Chem. Phys.* **16**, 2211–2223 (2014).
6. Hong, J. *et al.* A TCR mechanotransduction signaling loop induces negative selection in the thymus. *Nat. Immunol.* **19**, 1379–1390 (2018).
7. Hoffman, B. D., Grashoff, C. & Schwartz, M. A. Dynamic molecular processes mediate cellular mechanotransduction. *Nature* **475**, 316–323 (2011).
8. Hoekstra, T. P. *et al.* Switching between exonucleolysis and replication by T7 DNA polymerase ensures high fidelity. *Biophys. J.* **112**, 575–583 (2017).
9. Biebricher, A. S. *et al.* The impact of DNA intercalators on DNA and DNA-processing enzymes elucidated through force-dependent binding kinetics. *Nat. Commun.* **6**, 7304 (2015).
10. Dembo, M., Torney, D. C., Saxman, K. & Hammer, D. The reaction-limited kinetics of membrane-to-surface adhesion and detachment. *Proc. R. Soc. Lond. Ser. B Biol. Sci.* **234**, 55–83 (1988).
11. Sarangapani, K. K. *et al.* Low force decelerates L-selectin dissociation from P-selectin glycoprotein ligand-1 and endoglycan. *J. Biol. Chem.* **279**, 2291–2298 (2004).
12. Merkel, R., Nassoy, P., Leung, A., Ritchie, K. & Evans, E. Energy landscapes of receptor–ligand bonds explored with dynamic force spectroscopy. *Nature* **397**, 50–53 (1999).
13. Scheuermann, J., Viti, F. & Neri, D. Unexpected observation of concentration-dependent dissociation rates for antibody–antigen complexes and other macromolecular complexes in competition experiments. *J. Immunol. Methods* **276**, 129–134 (2003).
14. Hinterdorfer, P., Schilcher, K., Baumgartner, W., Gruber, H. J. & Schindler, H. A mechanistic study of the dissociation of individual antibody–antigen pairs by atomic force microscopy. *Nanobiology* **4**, 177 (1998).
15. Kulin, S., Kishore, R., Hubbard, J. B. & Helmerson, K. Real-time measurement of spontaneous antigen–antibody dissociation. *Biophys. J.* **83**, 1965–1973 (2002).
16. Dembo, M. On peeling an adherent cell from a surface. *Lect. Math. Life Sci.* **24**, (1994).
17. Bell, G. I. Models for the specific adhesion of cells to cells. *Science* **200**, 618–627 (1978).
18. Dahlke, K., Zhao, J., Sing, C. E. & Banigan, E. J. Force-dependent facilitated dissociation can generate protein–DNA catch bonds. *Biophys. J.* **117**, 1085–1100 (2019).
19. Nishizaka, T., Miyata, H., Yoshikawa, H., Ishiwata, S. & Kinosita, K. Unbinding force of a single motor molecule of muscle measured using optical tweezers. *Nature* **377**, 251–254 (1995).
20. Jannasch, A., Bormuth, V., Storch, M., Howard, J. & Schäffer, E. Kinesin-8 is a low-force motor protein with a weakly bound slip state. *Biophys. J.* **104**, 2456–2464 (2013).
21. Bormuth, V., Varga, V., Howard, J. & Schäffer, E. Protein friction limits diffusive and directed movements of kinesin motors on microtubules. *Science* **325**, 870–873 (2009).
22. Capitanio, M. & Pavone, F. S. Interrogating biology with force: Single molecule high-resolution measurements with optical tweezers. *Biophys. J.* **105**, 1293–1303 (2013).
23. Honarmandi, P., Lee, H., Lang, J. M. & Kamm, D. R. A microfluidic system with optical laser tweezers to study mechanotransduction and focal adhesion recruitment. *Lab Chip* **11**, 684–694 (2011).
24. Grashoff, C. *et al.* Measuring mechanical tension across vinculin reveals regulation of focal adhesion dynamics. *Nature* **466**, 263–266 (2010).
25. Bustamante, C., Alexander, L., Maciuba, K. & Kaiser, C. M. Single-molecule studies of protein folding with optical tweezers. *Annu. Rev. Biochem.* **89**, 443–470 (2020).

26. Smith, S. B., Cui, Y. & Bustamante, C. Overstretching B-DNA: The elastic response of individual double-stranded and single-stranded DNA molecules. *Science* **271**, 795–799 (1996).
27. Wang, M. D. *et al.* Force and velocity measured for single molecules of RNA polymerase. *Science* **282**, 902–907 (1998).
28. Evans, E. & Ritchie, K. Dynamic strength of molecular adhesion bonds. *Biophys. J.* **72**, 1541–1555 (1997).
29. Rao, L., Berger, F., Nicholas, M. P. & Gennerich, A. Molecular mechanism of cytoplasmic dynein tension sensing. *Nat. Commun.* **10**, 3332 (2019).
30. Nicholas, M. P. *et al.* Cytoplasmic dynein regulates its attachment to microtubules via nucleotide state-switched mechanosensing at multiple AAA domains. *PNAS* **112**, 6371–6376 (2015).
31. Andreasson, J. O. *et al.* Examining kinesin processivity within a general gating framework. *Elife* **4**, e07403 (2015).
32. Evans, E. Probing the relation between force—lifetime—and chemistry in single molecular bonds. *Annu. Rev. Biophys. Biomol. Struct.* **30**, 105–128 (2001).
33. Berger, F., Klumpp, S. & Lipowsky, R. Force-dependent unbinding rate of molecular motors from stationary optical trap data. *Nano Lett.* **19**, 2598–2602 (2019).
34. Uemura, S. *et al.* Kinesin–microtubule binding depends on both nucleotide state and loading direction. *PNAS* **99**, 5977–5981 (2002).
35. Trefethen, L. N. *Approximation Theory and Approximation Practice, Extended Edition*. (SIAM, 2019).
36. Corless, R. M. & Fillion, N. Polynomial and rational interpolation. in *A Graduate Introduction to Numerical Methods: From the Viewpoint of Backward Error Analysis* (eds. Corless, R. M. & Fillion, N.) 331–401 (Springer, 2013). https://doi.org/10.1007/978-1-4614-8453-0_8.
37. *Mathematica*. (Wolfram Research, Inc., 2021).
38. Pereverzev, Y. V., Prezhdo, O. V., Forero, M., Sokurenko, E. V. & Thomas, W. E. The two-pathway model for the catch-slip transition in biological adhesion. *Biophys. J.* **89**, 1446–1454 (2005).
39. Prezhdo, O. V. & Pereverzev, Y. V. Theoretical aspects of the biological catch bond. *Acc. Chem. Res.* **42**, 693–703 (2009).
40. Pereverzev, Y. V., Prezhdo, O. V., Thomas, W. E. & Sokurenko, E. V. Distinctive features of the biological catch bond in the jump-ramp force regime predicted by the two-pathway model. *Phys. Rev. E* **72**, 010903 (2005).
41. Rakshit, S., Zhang, Y., Manibog, K., Shafriz, O. & Sivasankar, S. Ideal, catch, and slip bonds in cadherin adhesion. *PNAS* **109**, 18815–18820 (2012).
42. Rico-Pasto, M., Pastor, I. & Ritort, F. Force feedback effects on single molecule hopping and pulling experiments. *J. Chem. Phys.* **148**, 123327 (2018).
43. Sonar, P. *et al.* Effects of ligand binding on the energy landscape of Acyl-CoA-binding protein. *Biophys. J.* **119**, 1821–1832 (2020).
44. Izadi, D. *et al.* Combined force ramp and equilibrium high-resolution investigations reveal multipath heterogeneous unfolding of protein G. *J. Phys. Chem. B* **122**, 11155–11165 (2018).
45. Capitanio, M. *et al.* Ultrafast force-clamp spectroscopy of single molecules reveals load dependence of myosin working stroke. *Nat. Methods* **9**, 1013–1019 (2012).
46. *MATLAB*. (The MathWorks, Inc., 2021).
47. Gillespie, D. T. A general method for numerically simulating the stochastic time evolution of coupled chemical reactions. *J. Comput. Phys.* **22**, 403–434 (1976).
48. Phillips, R., Kondev, J. & Theriot, J. *Physical Biology of the Cell* (Garland Science, 2013).

Acknowledgements

A.P. was supported by a Clemson Research Fellows R-Initiative Award from Clemson University. This work was supported by the National Institute of Allergy and Infectious Diseases (NIAID) of the National Institutes of Health under award number R15AI137979, by the National Institute of General Medical Sciences (NIGMS) of the National Institutes of Health under award number P30 GM131959, and by Clemson University. We would like to thank Ashok Pabbathi for his sample data (Figure 1b) and Ashok Pabbathi and Subash Godar for their insightful discussions. Additionally, we thank Marija Zanic for reading and commenting on early drafts of the manuscript.

Author contributions

A.P. and J.A. contributed to the conceptualization of the study, performed the analytical and computational work, analyzed the results, and revised the manuscript. A.P. drafted the first draft of the manuscript. J.A. supervised the project.

Competing interests

The authors declare no competing interests.

Additional information

Supplementary Information The online version contains supplementary material available at <https://doi.org/10.1038/s41598-021-03690-1>.

Correspondence and requests for materials should be addressed to J.A.

Reprints and permissions information is available at www.nature.com/reprints.

Publisher's note Springer Nature remains neutral with regard to jurisdictional claims in published maps and institutional affiliations.



Open Access This article is licensed under a Creative Commons Attribution 4.0 International License, which permits use, sharing, adaptation, distribution and reproduction in any medium or format, as long as you give appropriate credit to the original author(s) and the source, provide a link to the Creative Commons licence, and indicate if changes were made. The images or other third party material in this article are included in the article's Creative Commons licence, unless indicated otherwise in a credit line to the material. If material is not included in the article's Creative Commons licence and your intended use is not permitted by statutory regulation or exceeds the permitted use, you will need to obtain permission directly from the copyright holder. To view a copy of this licence, visit <http://creativecommons.org/licenses/by/4.0/>.

© The Author(s) 2022